Supporting Information

Molecular-level Anchoring Polymer Cathodes on Carbone Nanotubes

towards Rapid-Rate and Long-Cycle Sodium-Ion Storage

Yuxiang Hu[a,b],‡ Kai Zhang[b],‡ Han Hu[a,b], Songcan Wang[a,b], Delai Ye[a,b], Michael J. Monteiro [b], Zhongfan Jia[b],*, and Lianzhou Wang[a,b],*

[a.] Nanomaterials Centre, School of Chemical Engineering, The University of Queensland, QLD 4072, Australia.

[b.] Australian Institute for Bioengineering and Nanotechnology, The University of Queensland, QLD 4072, Australia. E-mail: l.wang@uq.edu.au; z.jia@uq.edu.au
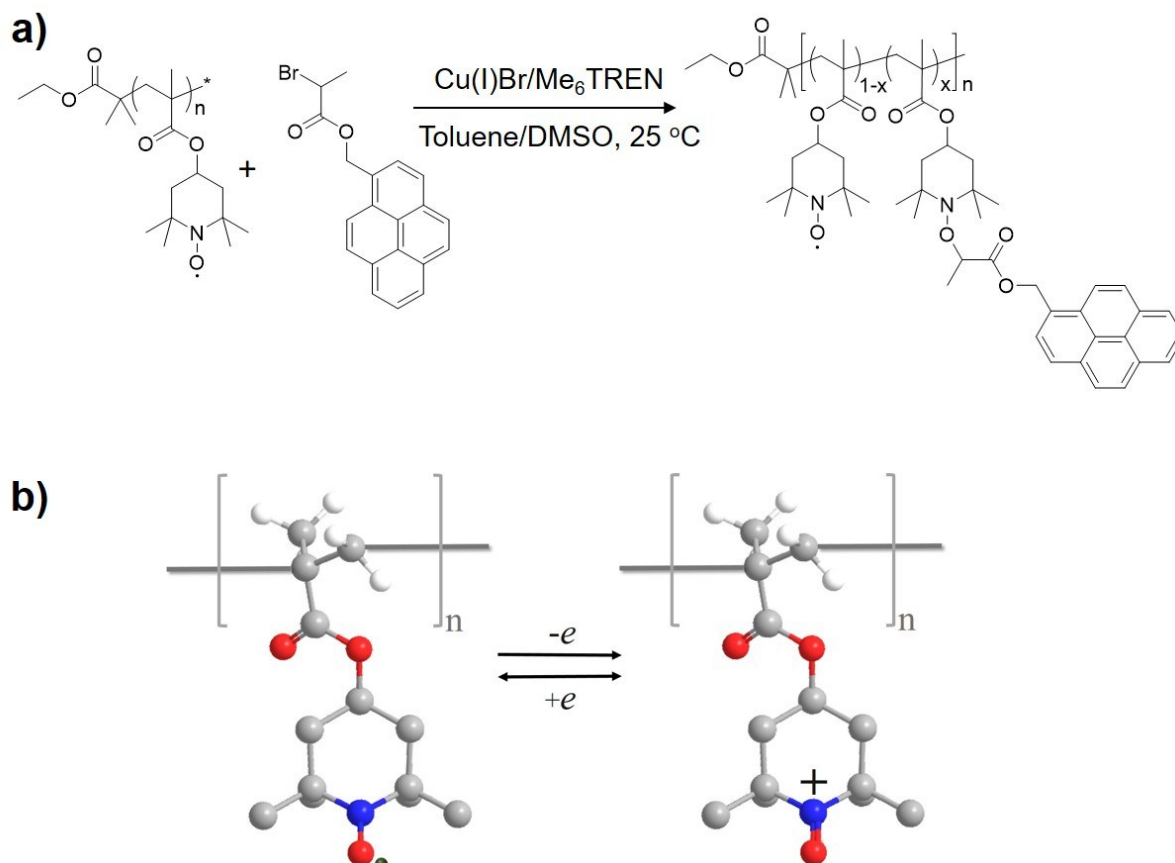
Figure S1. a) The functionalization of the PTMA with pyrene group was carried out via nitroxide radial coupling (NRC) click reaction.[1] Briefly, pyren-1-ylmethyl 2-bromopropanoate was firstly reacting with Cu(I) to generate a high active carbon radical after losing the bromide, which was quickly coupled by the nitroxide radical in a diffusion controlled manner to form a stable C-O bond with quantitative conversion under ambient conditions.[2] The pyrene group, which is commonly applied poly-cyclic aromatic compounds, along the PTMA chain would have noncovalent π to π stacking interaction with the CNTs. This π-π interaction will anchor polymer on the surface of the CNTs matrix. b) Schematic diagram of the electrochemical mechanism of PTMA. TEMPO radicals on PTMA act as both chemical reactive functionalities for NRC reaction and redox-active groups for energy storage, which, in the latter case, TEMPO radicals undergo a reversible oxidation and form oxoammonium cations.
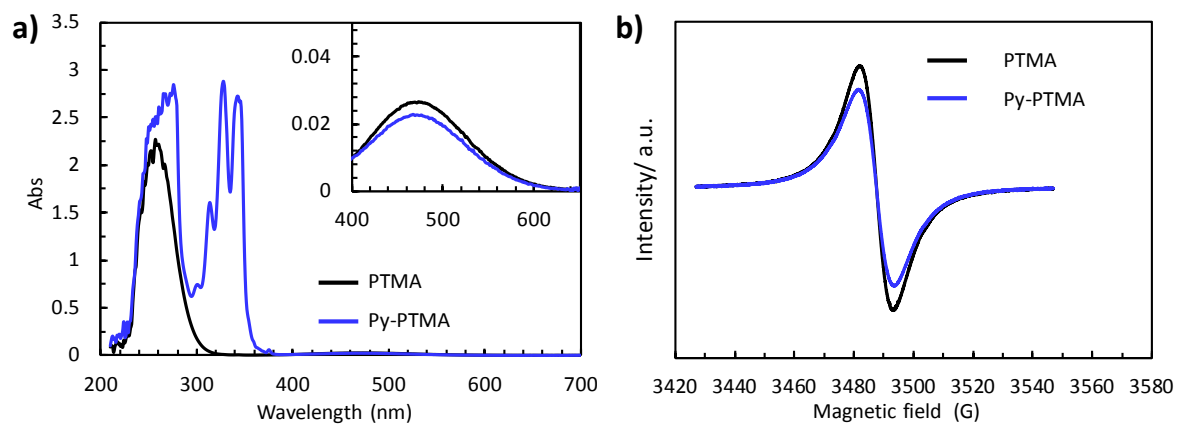
Figure S2. (a) UV-Vis spectrum of PTMA and Py-PTMA with inset showing the enlarged spectra assignable to the n-π* adsorption of nitroxide radicals. (b) EPR of PTMA and Py-PTMA.
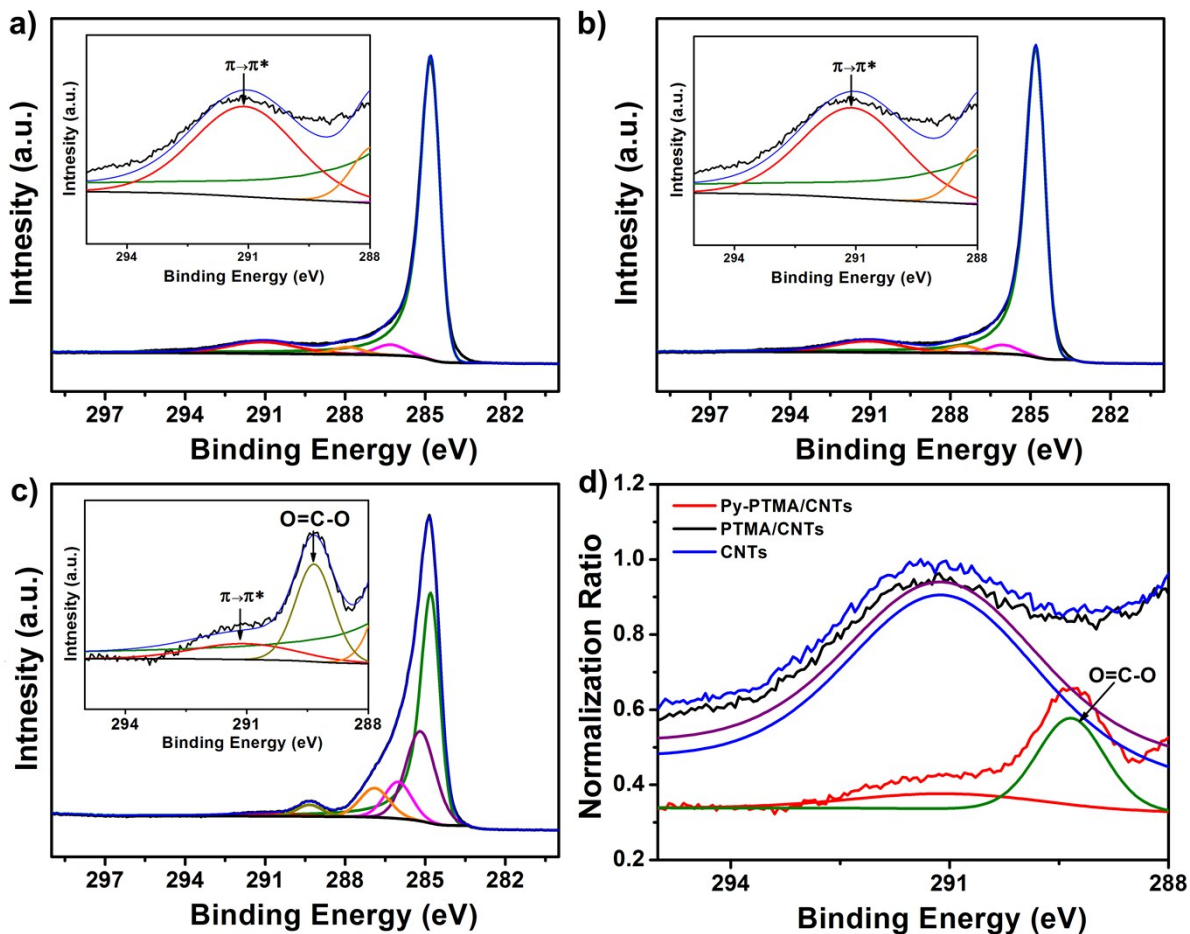
Figure S3. XPS spectra of C 1s in a) CNTs, b) PTMA/CNTs and c) Py-PTMA/CNTs with the amplified area around 291 ev in the inset. d) Normalized XPS spectra of the three samples with the binding energy around 291 eV based on the highest intensity in the spectra from 288 to 295 eV. The additional peak in the peak fitting of Fig. S3c was ascribed to the C in the Py-PTMA in comparison with that of Fig. S3a. For example, the small peak between 290 eV and 285 eV (Fig. S3c) would ascribe to the C 1s of O-C=O from the polymer.[3] The O-C=O group could be observed in the molecular of Py-PTMA in Fig. S1a. Owing to the detection area and the heterogeneous distribution of PTMA/CNT, the polymer signal of PTMA/CNT spectra (Fig. S3b) was no obvious. The typical peak related to the π→π∗ transition of C 1s, which is commonly observed in CNTs around 291 eV, could be easily observed in XPS spectra of CNTs and PTMA/CNTs. However, the C 1s spectra of Py-PTMA/CNTs mainly displayed weak π→π∗ transition peak around 291 eV, which further prove the uniformity Py-PTMA sheath on the surface of CNTs. Note that, the π-π stacking interaction between pyrene and

4

CNTs is not the chemical bonding, which is different from the $\pi \rightarrow \pi*$ transition of CNTs. The coated polymer sheath reduced the typical signal of the inside CNTs with the weaker $\pi \rightarrow \pi*$ transition and the higher typical signal from the polymer.
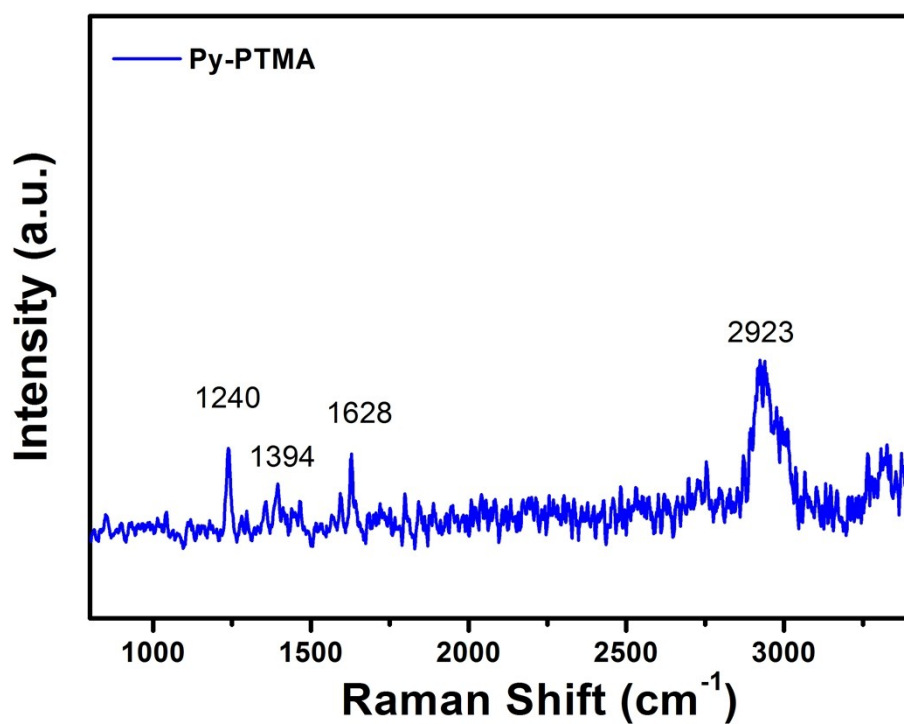
Figure S4. Raman spectra of Py-PTMA with characteristic peaks after baseline correction. Compared with the high intensity of that of CNTs, the intensity of Py-PTMA is not that high. Although the peaks from 1200 cm^{-2} to 1700 cm^{-2} are among the characteristic peaks of the CNTs, the weak characteristic peaks did not disturb the characteristic peaks of Py-PTMA/CNT. Due to the intensity variation, the Raman spectra of CNTs mostly contributes to the final Raman spectra of Py-PTMA.
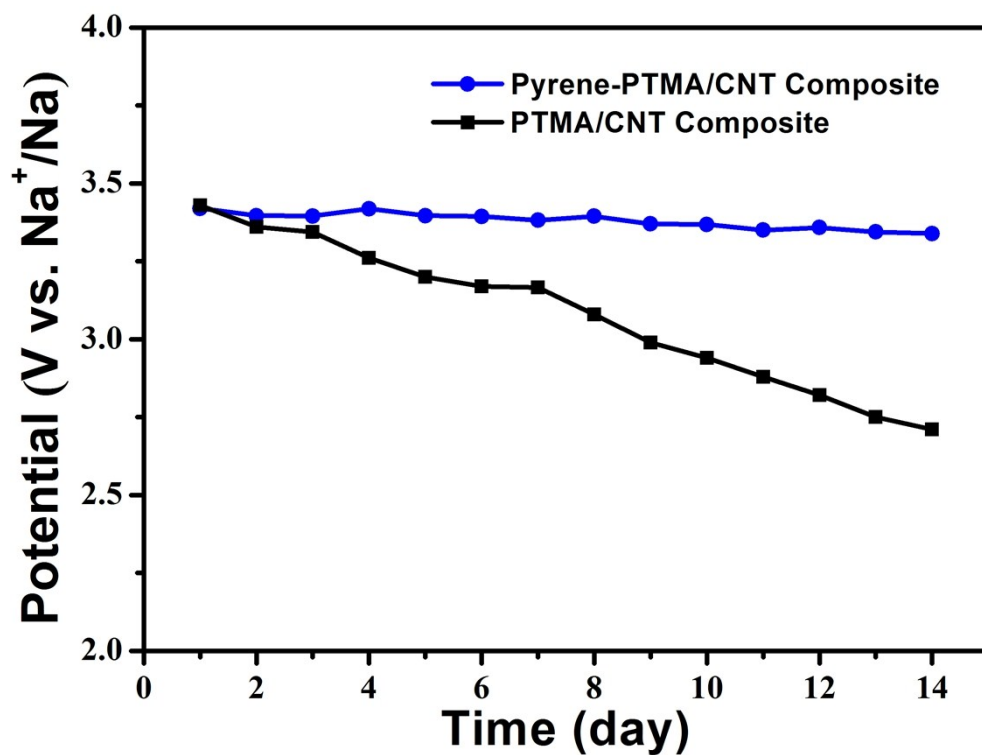
Figure S5. After fully charged to 3.7 V (vs. Na$^+$/Na), open circuit voltage curves of the Py-PTMA/CNTs (bule) and normal PTMA/CNTs composite (dark) electrode-based sodium battery during the two weeks measurment period.
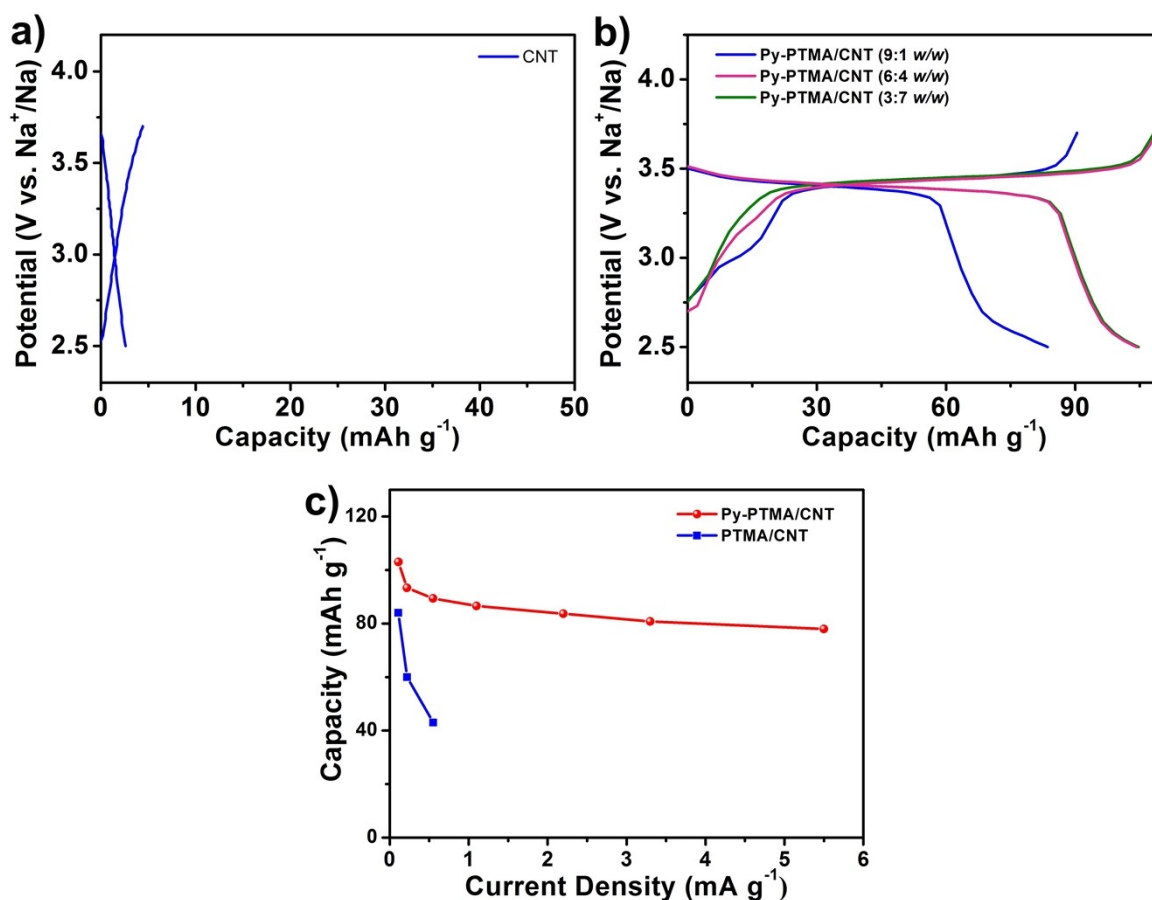
Figure S6. a) The CNTs capacity in the testing voltage range. b) The charge-discharge capacity of the Py-PTMA/CNT under different weight ratios (9:1, 6:4, and 3:7) at the current density of 1 C-rate. c) Rate-performance of the Py-PTMA/CNT and PTMA/CNT. Based on the Fig. S6a), the CNTs contribute a negligible capacity to the overall capacity of Py-PTMA/CNT. The CNTs ratio was optimized with the different weight ratio in Fig. S6b). If the CNTs weight ratio is too low (9:1), the conductivity of whole Py-PTMA/CNT is inferior with inferior electrochemical performance. Although the higher weight content of the CNTs (3:7) would increase the conductivity, the ratio of active material would be less with lower whole energy density and capacity. Compared with the Py-PTMA/CNT, the capacity decayed quickly with increasing current density in the simple mixture of PTMA and CNTs electrode.

Table S1. Comparison with other representative polymer cathodes in SIBs

|	Sodium poly(pyrrole-co-(sodium-3-(pyrrollyl) propanesulphonate)) [4]	poly(diphenyla minesulfonic acid sodium) [5]	PTMA with nano-fibers [6]	Oligopyr ene [7]	**Our Material (Py-PTMA/CNTs)**	
Current Density (A g^{-1})	0.04	0.05	0.05	0.02	**0.11**	**2**
Capacity Retention (%)	84% after 100 cycles	70% after 100 cycles	64% after 50 cycles	69% after 100 cycles	**98% after 100 cycles**	**92% after 6000 cycles**
Capacity (mAh g^{-1}) after cycled	72	70	45	83	**105**	**78**
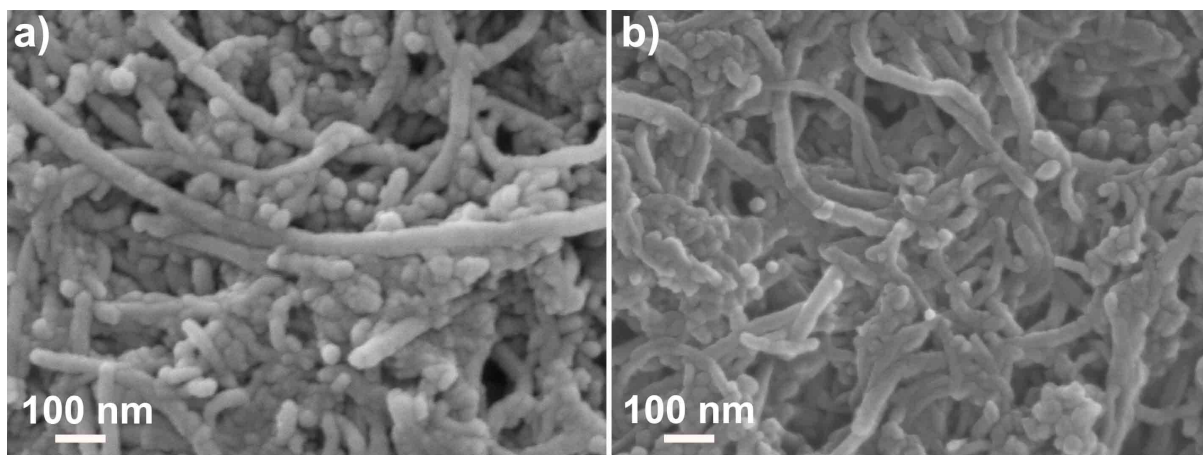
Figure S7. SEM images of the Py-PTMA/CNTs electrodes after (a) 600 and (b) 6000 cycles.
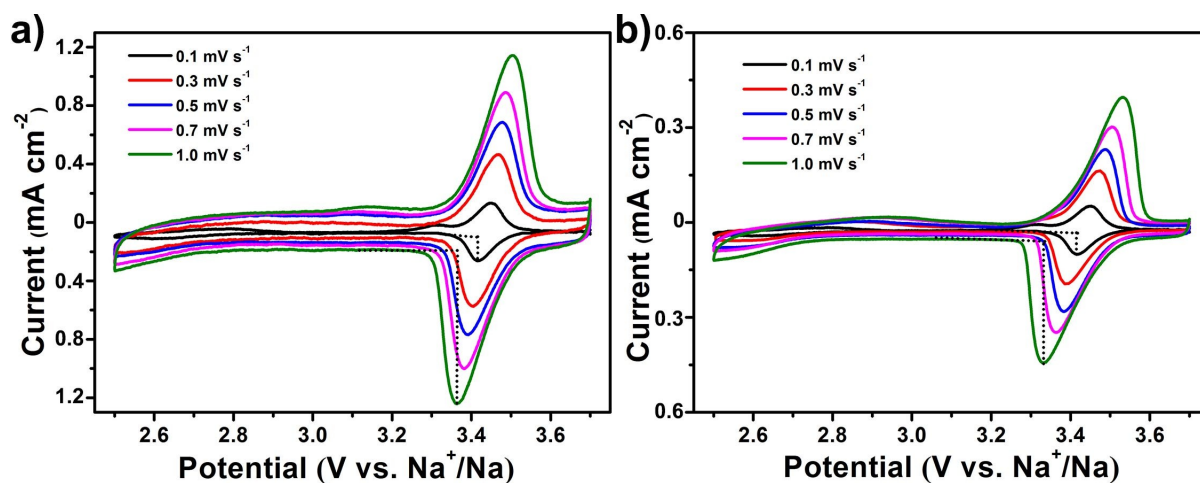
Figure S8. CV curves of (a) Py-PTMA/CNTs, and (b) PTMA/CNTs electrodes at different scan rate from 0.1 mV s^{-1} to 1.0 mV s^{-1}. The varied locations of the peak current in CV is ascribed to the over-potential at different scan rate, which has been proved in pristine literature.[8, 9] The dotted line in the figures showed the baseline corrections before the calculation of peak current density. In the meanwhile, the line of peak current density vs. square root of scan rate did not exactly across the original point was mainly ascribed to the no-optimal experiment condition, which has been also commonly shown in other similar works.[8, 10]
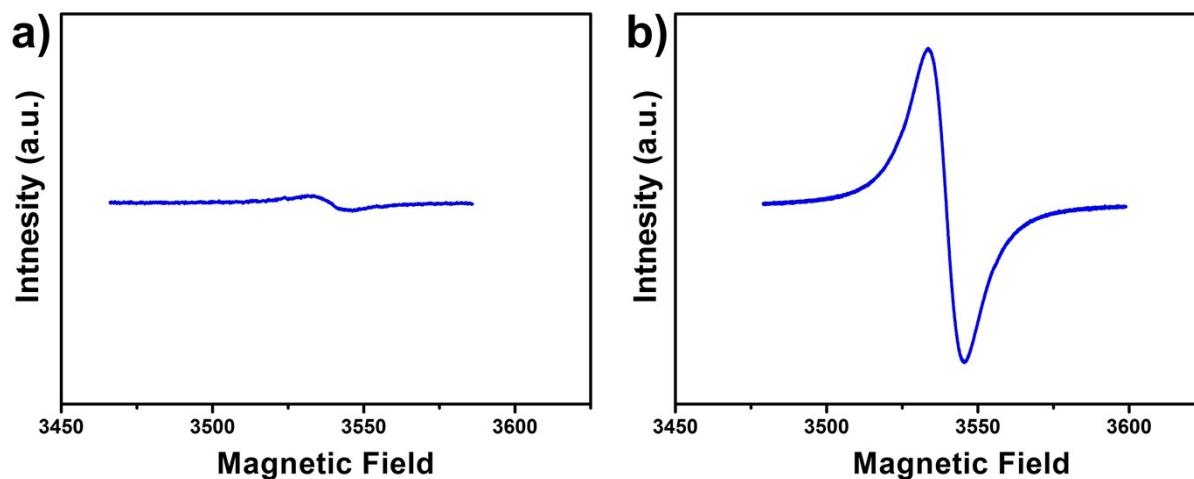
Figure S9 Electron paramagnetic resonance (EPR) of (a) fully charged and (b) fully discharged Py-PTMA/CNTs electrodes.

References:

1.   K. Zhang, Y. Hu, L. Wang, M. J. Monteiro and Z. Jia, *ACS Appl. Mater. Interfaces*, 2017, **9**, 34900-34908.
2.   J. Kulis, C. A. Bell, A. S. Micallef, Z. Jia and M. J. Monteiro, *Macromolecules*, 2009, **42**, 8218-8227.
3.   P. Cools, E. Sainz‑García, N. D. Geyter, A. Nikiforov, M. Blajan, K. Shimizu, F. Alba‑Elías, C. Leys and R. Morent, *Plasma Process. Polym.*, 2015, **12**, 1153-1163.
4.   L. Zhu, Y. Shen, M. Sun, J. Qian, Y. Cao, X. Ai and H. Yang, *Chem. Commun.*, 2013, **49**, 11370-11372.
5.   Y. F. Shen, D. D. Yuan, X. P. Ai, H. X. Yang and M. Zhou, *Electrochem. Commun.*, 2014, **49**, 5-8.
6.   Y. Dai, Y. Zhang, L. Gao, G. Xu and J. Xie, *Electrochem. Solid-State Lett.*, 2010, **13**, A22.
7.   S. C. Han, E. G. Bae, H. Lim and M. Pyo, *J. Power Sources*, 2014, **254**, 73-79.
8.   M. Burgess, K. Hernandez-Burgos, K. J. Cheng, J. S. Moore and J. Rodriguez-Lopez, *Analyst*, 2016, **141**, 3842-3850.
9.   R. Muruganantham, Y.-T. Chiu, C.-C. Yang, C.-W. Wang and W.-R. Liu, *Sci. Rep.*, 2017, **7**, 14808.
10.   W. Song, X. Ji, Y. Yao, H. Zhu, Q. Chen, Q. Sun and C. E. Banks, *Phys. Chem. Chem. Phys.*, 2014, **16**, 3055-3061.